Journal of Materials Chemistry A

Accepted Manuscript

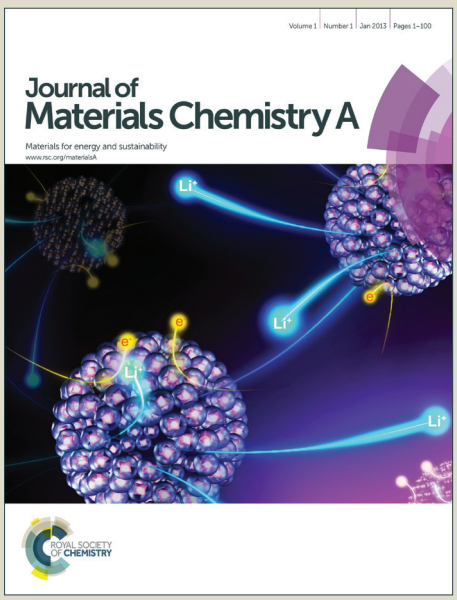

ROYAL SOCIETY OF CHEMISTRY

www.rsc.org/materialsA

Journal of Materials Chemistry A

Dynamic Article Links ►

Cite this: DOI: 10.1039/c0xx00000x

ARTICLE TYPE

www.rsc.org/xxxxxx

Facile construction of ultrathin standing α-Ni(OH)$_2$ nanosheets on halloysite nanotubes and its enhanced electrochemical capacitance

Jin Liang,[a] Bitao Dong,[a] Shujiang Ding,[a*] Cuiping Li,[b*] Ben Q Li,[c] Jun Li[d] and Guang Yang[e]

Received (in XXX, XXX) Xth XXXXXXXXX 200X, Accepted Xth XXXXXXXXX 200X

DOI: 10.1039/b000000x

One-dimensional nanostructure of ultrathin standing α-Ni(OH)$_2$ nanosheets@halloysite nanotubes is synthesized through one-step facile precipitation method. The nanocomposites exhibit high capacitance (1677 F g^{-1}) and excellent cycling stability (100 % capacity retention after 2000 cycles) due to their ultrathin and standing nanosheets and intense cation/anion exchange performance of halloysite nanotubes. The remarkable electrochemical performance will undoubtedly make the hybrid structures attractive for high-performance supercapacitors.

1. Introduction

The ever-growing demand for environmental protection and energy-intensive applications has stimulated reinforced research interest in energy storage and conversion from alternative energy sources.[1-5] So far, as one of the most ideal candidates for green energy storage devices, supercapacitors have been wildely studied on account of their long and stable cycle life, short charging time, high power density, low maintenance cost and minimal safety concerns.[6-8] On account of their intriguing electrochemical properties, supercapacitors can be used for momentary energy smoothing load services such as emergency power supplies and peak power assistance for batteries in electric vehicles.[9] However, the practical applications of supercapacitors have been intensively hampered by the inherent drawbacks of the existing electrode materials, such as the high cost of the RuO_2 based materials, relatively low specific capacitance of the carbon based materials and the poor cycling stability of the pseudocapacitive materials.[10-15] Nickel hydroxide has been studied as a high performance electrode materail for supercapacitors owning to its low fabraction cost, well defined electrochemical behaviors, flexible synthesis method and high theoretical capacity (3750 F g^{-1} at the voltage window of 0 and 0.5 V).[16-20] However, nickel hydroxide based materials rely on Faradic redox reactions and thus can not support fast transport of electrons. The energy storing mechanisms for nickel hydroxide is described by the redox reaction (1),

$$\alpha - Ni(OH)_2 + OH^- \leftrightarrow \gamma - NiOOH + H_2O + e^- \quad (1)$$

Clearly, the reaction represents a compromise of rate capability and reversibility. It is known that the rate capability of electrode materials is determined mainly by the rate of ion diffusion and the electronic conductivity. The latter is often accomplished by using conductive substrate (such as carbon nanofibers and nanotubes, Ni foam et al) to enhance the conductivity of the active materials.[15, 21-23] According to reaction (1), the hydroxyl ion plays an important role and hence the rate capability of the supercapacitors can be enhanced through the increase of the ionic conductivity.

Halloysite (HA), a kind of one-dimensional tubular clay minerals, has versatile features, such as high porosity, tunable surface chemistry and low cost.[24-26] In addition, it possesses excellent cation/anion exchange capacity and abundant OH^- on the surface, which is highly possible to enhance the diffusion rate of OH^-, thus enhancing the rate capability of nickel hydroxide based materials.

In this work, we employ a one-step facile low-temperature precipitation method to construct 1D α-Ni(OH)$_2$ nanosheets@HA nanotubes hybrid nanostructures.[27] The as-prepared α-Ni(OH)$_2$@HA composites are unusually suitable as the electrode materials for supercapacitors for at least three reasons: i) These hierarchical and ultrathin α-Ni(OH)$_2$ nanosheets could offer rich accessible electroactive sites, short ion transport pathways, superior electron collection efficiency and buffer the large volume change during the fast charging–discharging process;[28] ii) t

he standing structure may help to the separation of neighboring nanosheets, thus restraining the active material from aggregating; iii) the remarkable cation/anion exchange capacity of HA nanotubes can offer quick and sustainable supply or removal of participant ions during the charge-discharge process, which can be considered as fascinating synergetic properties, thus enormously enhancing the rate capability of α-Ni(OH)$_2$ nanosheets@HA nanotubes. In terms of the above-mentioned advantages, the integrated hybrid electrodes exhibit an excellent specific capacitance and cycling stability even at a high charge/discharge current density.

2. Experimental

2.1 Materials

The halloysite (HA) nanotubes were purchased from Imerys Tableware Asia Limited. The chemicals, polyvinylidene fluoride (PVDF) and N-methyl-2-pyrrolidone (NMP), were purchased from Sigma-Aldrich. All reagents were analytical grade and used without further purification.

2.2 The synthesis of α-Ni(OH)$_2$ aggregates and α-Ni(OH)$_2$ nanosheets@HA nanotubes

5 mg of halloysite (HA) nanotubes was well dispersed in 40 mL of deionized water by sonication treatment. Then, 0.25 mmol of $Ni(NO_3)_2 \cdot 6H_2O$, 0.25 mmol of hexamethylenetetramine and 0.025 mmol of citric acid trisodium salt dehydrate were dissolved into the above dispersion to form a light green solution. The resulting solution was then heated to 90 ^oC in an oil bath for 6 h with slow stirring. After the solution was cooled down to room temperature naturally, the product was collected by centrifugation and washed with deionized water and ethanol several times. α-Ni(OH)$_2$@HA was finally obtained after being dried in a vacuum at 60 ^oC for 12 h. α-Ni(OH)$_2$ aggregates were prepared via a similar procedure without halloysite. The synthetic process is illustrated in Scheme 1.

2.3 Materials characterization

X-ray diffraction (XRD) patterns were collected on a SHIMADZU Lab X X-6000 Advanced X-Ray Diffractometer. IR spectra were obtained on a Bruker RENSOR27 Fourier transform infrared (FT-IR) spectrometer ranged from 4000 to 400 cm^{-1}. The samples and KBr crystal were ground together, and then the mixture was pressed into a flake for IR spectroscopy. The chemical states of the products were studied using the X-ray photoelectron spectroscopy (XPS) measurement performed on an Axis Ultra, Kratos (UK) at monochromatic Al K a radiation (150 W, 15 kV and 1486.6 eV). The vacuum in the spectrometer was 10–9 Torr. Binding energies were calibrated relative to the C 1s peak (284.6 eV). Field-emission scanning electron microscope (FESEM) images were obtained on a HITACHI SU-8010 microscope. Transmission electron microscope (TEM) images were taken on a JEOL JEM-2100 microscope. Thermogravimetric analysis (Perkin-Elmer TGA 7) was carried out under a flow of air with a temperature ramp of 10 $^oC\ min^{-1}$ from room temperature to 800 ^oC.

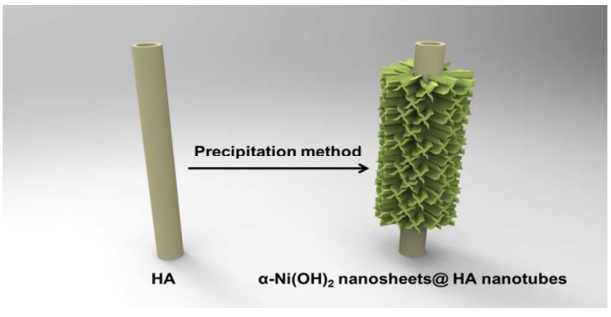

Scheme 1. Schematic illustration of the synthetic procedure of Ni(OH)$_2$ nanosheets@HA nanotubes hybrid nanostructures.

2.4 Electrochemical measurements

For electrochemical measurements, the working electrode was consisted of an active material, carbon black (TIMICAL SUPER C65), and a polymer binder in a weight ratio of 70:20:10. The polymer binder was self-prepared by dissolving commercial PVDF powder into NMP solvent with a weight ratio of 7:93. The as-prepared slurry was then pasted onto graphite paper and dried at 60 ^oC at oven for 8 h and following at 120 ^oC overnight under vacuum. The electrochemical test was conducted with a electrochemical workstation (CHI 660D) in an aqueous KOH electrolyte (2.0 M) with a three-electrode cell where Pt foil serves as the counter electrode and a saturated calomel electrode (SCE) as the reference electrode.

3. Result and discussion

3.1 Material characterizations

A commercial halloysite nanotubes are selected as substrate for preparing the 1D α-Ni(OH)$_2$ nanosheets@HA hybrid nanostructure. Morphology and structure of HA nanotubes have been characterized with SEM and TEM. As shown in Fig. 1A, the halloysites predominately consiste of cylindrical nanotubes 50-150 nm in diameter and 1-2 μm in length.[25] The empty limen structure of HA is revealed by TEM image. As shown in Fig. 1B, the average inner diameter of the HA is in the range of 40-60 nm. The aggregates of α-Ni(OH)$_2$ without HA supportting is also prepared as compared sample in the similar procedure, and the morphology was shown in Fig. 1C and 1D. It is apparent that α-Ni(OH)$_2$ aggregates possess a chain morphology composed of irregular spheres with a diameter of ~1μm. After further careful observation, the irregular spheres are composed of thin nanosheets. The morphology of α-Ni(OH)$_2$ nanosheets@HA nanotubes has been confirmed with SEM and TEM images (Fig. 2). As seen in Fig. 2A, a large amount of uniform 1D nanostructures are obtained with a hierarchical architecture. From an enlarged view of the FESEM image (Fig. 2B), these 1D nanostructures are composed of uniform α-Ni(OH)$_2$ nanosheets grown

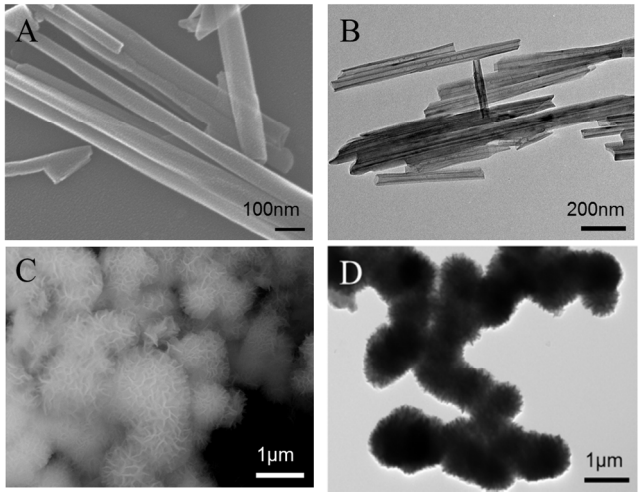

Fig. 1 SEM (A) and TEM (B) images of the halloysite (HA) nanotubes; SEM (C) and TEM (D) images of α-Ni(OH)$_2$.

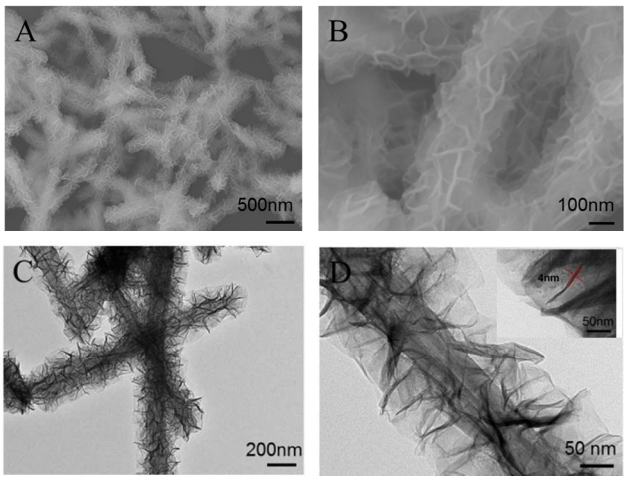

Fig. 2 SEM images (A, B) and TEM images (C, D) of the ultrathin standing α-Ni(OH)$_2$ nanosheets@HA nanotubes.

surrounding the surface of HA nanotubes. In addition, the nanosheets show a hierarchical array feature with empty space among adjacent nanosheets. This feature could benefit the penetration of the electrolyte, which may contribute to improve electrochemical performance. It can be clearly observed (Fig. 2C) that α-Ni(OH)$_2$ nanosheets are grown rather uniformly and surroundding the HA nanotubes to form the 1D structure. An enlarged view (Fig. 2D) provides the evidence that the standing α-Ni(OH)$_2$ nanosheets are chemically grown on the HA nanotubes, which could be derived from the self-seeded growth process. The length of nanosheets is about 200 nm and the thicknessis approximate 4 nm (the inset in Fig. 2D). The nanosheets would promote more ions to participate in the reaction and increase the availability of the nanomaterials to enhance the energy density. All above, the well defined α-Ni(OH)$_2$@HA nanostructures can be prepared by this low-cost effective precipitation route. The thermal behavior is estimated by the thermogravimetric analysis (TGA) (Fig. 3a). Curve (I) shows that adsorbed water and interlayer water are removed in the first stage of this process (up to 60 °C), the thermal decomposition of HA is completed at 450 °C. This weight loss can be vested as a continuous thermal depletion of deep-trapped hydroxyl groups and inherent moisture. Curve (III) indicates that while trapped moisture can be removed in the early stage of this process (up to 100 °C), the thermal decomposition of α-Ni(OH)$_2$ is intensively completed at 300 °C. The weight loss over 300 to 800 °C can be assigned to a continuous thermal depletion of deep-trapped hydroxyl groups and removal of chemisorbed carbonate anions. Curve (II) displays the thermal decomposition of α-Ni(OH)$_2$@HA hybrid nanostructures with two apparent weight loss. Using Energy Dispersive X-ray Spectrom (EDS) (Fig. 3b), we calculate that the mass fraction of α-Ni(OH)$_2$ is esimated to be about 45% in the hybrid nanostructures.

The X-ray diffraction (XRD) is used to further confirm the crystal structure and composition of the hybrid structure. Fig. 4 shows the patterns of HA, α-Ni(OH)$_2$@HA and α-Ni(OH)$_2$. Curve (a) apparently reveals the main four characteristic diffraction peaks at 24.6^o, 33.4^o, 34.9^o and 59.7^o corrensponding to the (006), (101), (012) and (110) of α-Ni(OH)$_2$, which is in good agreement with standard power diffraction patterns of α-Ni(OH)$_2$ (JCPDS No. 38-0715).[29, 30] The diffraction peaks confirm the high crystallinity of the as-prepared material. Meanwhile, some crystal face of halloysite nanotubes, such as (002), (110), (003), (211) at 24.84^o, 35.02^o, 37.98^o and 54.34^o appear (curve c). Curve (b) indicates that the hybrid materials synchronously possess the characteristic diffraction peaks of HA and α-Ni(OH)$_2$, confirming the composition of the hybrid materials.

The chemical structure of as-prepared composites is further characterized by Fourier transform IR (FT-IR). Curve a in Fig. 5a shows the characteristic bands of halloysite, such as the stretching vibration of the inner-surface hydroxyl groups of Al_2OH at 3695 and 3620 cm^{-1}, the deformation vibration of the above hydroxyl groups at 910 cm^{-1}, and the deformation vibration of Al–O–Si and Si–O–Si at 538 and 469 cm^{-1}.[25, 31, 32] The reactions of the FT-IR spectra (Fig. 6b, Curve b) indicate that the structure of halloysite nanotubes remaine unaffected by the Ni(OH)$_2$-treatment except the Si–O broad stretching band at about 1029 cm^{-1}, which shifted to 1031 cm^{-1} for α-Ni(OH)$_2$@HA. The shifting of the Si–O broad stretching band indicates the formation of hydrogen bonding between the outer surface of the halloysite nanotubes and α-Ni(OH)$_2$. The new bands at 3490 and 1624 cm^{-1} are most likely due to the stretching vibration and the corresponding deformation vibration of the hydroxyl groups involve in hydrogen bonding, which come from absorbed H_2O and hydroxyl groups interacting with adsorbed species. Two strong bonds at 1369 and 632cm^{-1} are observed, which can be attributed to the vibration of the interbedded NO_3- groups of α-Ni(OH)$_2$ and Ni–O–H bending vibrations, respectively.

More detailed elemental composition and the oxidation state of the as-prepared composites are further investigated using X-ray photoelectron spectroscopy (XPS) and the corresponding results are presented in Fig. 6. The survey spectrum (0-1200 eV) (Fig. 6a) of α-Ni(OH)$_2$@HA nanosheets shows mainly carbon (C 1s), oxygen (O 1s) and nickel species.[33] The binding energies for Si 2p, Al 2p, O 1s, and C 1s are 104.4, 70.4, 529, and 282 eV, respectively.[23] In the Ni 2p binding energies at 853.3 and 870.9 eV, corresponding to Ni 2p3/2 and Ni 2p1/2, respectively, with a spin-energy separation1s are 104.4, 70.4, 529, and 282 eV,

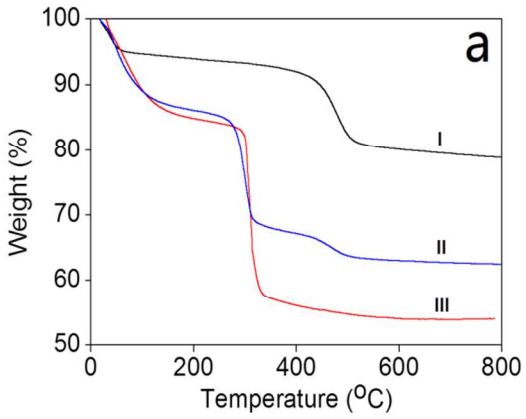

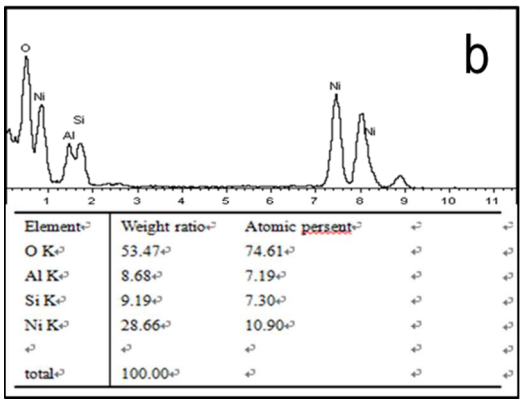

Element	Weight ratio	Atomic persent
O K	53.47	74.61
Al K	8.68	7.19
Si K	9.19	7.30
Ni K	28.66	10.90
total	100.00	

Fig. 3 (A) TGA analysis of HA nanotubes (I), α-Ni(OH)$_2$ nanosheets@HA (II) and α-Ni(OH)$_2$ nanosheets (III) under air flow with a temperature ramp of 10 ^{o}C min^{-1}; EDS (B) of α-Ni(OH)$_2$ nanosheets@HA nanotubes.

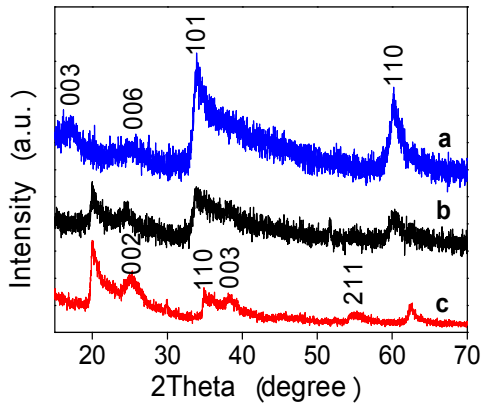

Fig. 4 XRD patterns of α-Ni(OH)$_2$ aggregates (a), α-Ni(OH)$_2$ nanosheets@HA (b) and HA nanotubes (c).

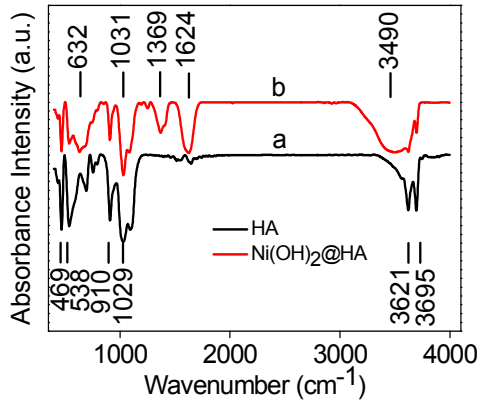

Fig. 5 FT-TR spectra of pure HA nanotubes and α-Ni(OH)$_2$ nanosheets@HA nanotubes.

respectively. In the Ni 2p region (Fig. 6b), the spectrum shows two major peaks with binding energies at 853.3 and 870.9 eV, corresponding to Ni 2p3/2 and Ni 2p1/2, respectively, with a spin-energy separation of 17.6 eV, which is characteristic of Ni(OH)$_2$ phase and in good agreement with the literature.[34, 35] In addition, The satellite peak at around 859.0 eV and 877.4 eV are two shake-up type peaks of nickel at the high binding energy side of the Ni 2p3/2 and Ni 2p1/2 edge.[34]

3.2 Electrochemical characterizations

It will be interesting to evaluate the electrochemical performance of the synthesized materials as electrodes for supercapacitors. The CV curves of α-Ni(OH)$_2$@HA nanostructure electrode with various sweep rates ranging from 3 to 30 mV s^{-1} are shown in Fig. 7(a), which consists of a pair of redox peaks within the potential range from 0 to 0.55 V vs. SCE and reveals the pseudocapacitive characteristics. This is owing to the reversible reduction as described by reaction (1). Such a peak potential difference can be regarded as quasi-reversible. The shape of the CV curves was basically constant at different scan rates, which resultes from the improved mass transportation within the electrode materials.[36] The Fig. 7(b) shows the galvanostatic discharge profiles at different current densities ranging from 6 to 30 A g^{-1}. The specific capacitance is calculated by the formula,

$$C_m = I * \Delta t/(\Delta V * m) \quad (2)$$

Where C$_m$ (F g^{-1}) is the specific capacitance, I is the discharge current, Δt is the discharge time, ΔV is the voltage range and m is the mass of the active material (i.e., the total mass of the hybrid nanostructure). The calculated specific capacitance as a function of the discharge current density is plotted in Fig. 7(c). It is seen that the specific capacitance is as high as 1255, 1493, 1630, 1677 and 1771 F g^{-1} at discharge current densities of 30, 20, 15, 10 and 6 A g^{-1}, respectively. In addition, the cycling stability is also evaluated by the repeated charging-discharging measurement at a

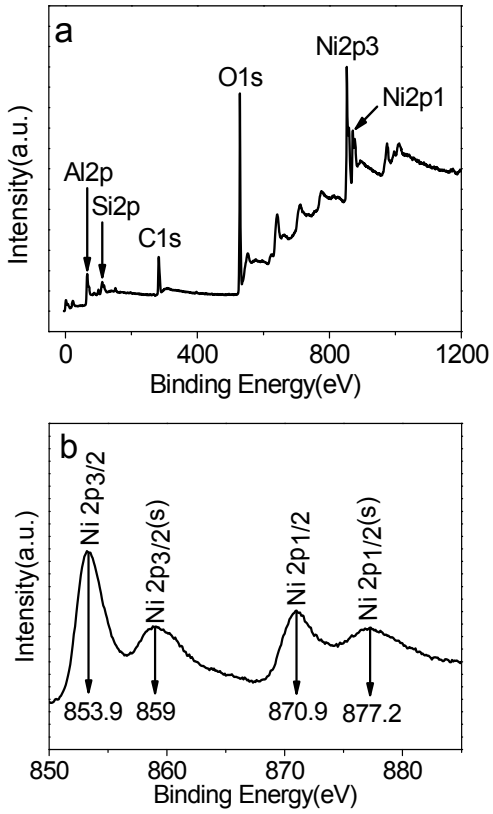

Fig. 6 (a) XPS survey spectrum of α-Ni(OH)$_2$@HA sample and (b) Ni 2p core level.

constant current density of 10 A g^{-1}, as shown in Fig. 7(d) (I). The specific capacitance is around 1688 F g^{-1} in the first cycle and it gradually increases to1751 F g^{-1} after cycling for 400 cycles. Subsequently, the capacitance is keeping at 1688 F g^{-1}. This corresponds to no any capacitance loss, which is considered a reasonably good performance for metal hydroxide nanostructures based electrode materials. Comparison of the cycling performances of α-$Ni(OH)_2$ aggregates and HA nanotubes are shown in Fig. 7(d) (II and III) indicates that α-$Ni(OH)_2$@HA hybrid nanostructure possesses the miraculously high specific capacitance. The capacity is also higher than some $Ni(OH)_2$-based materials, which have a capacitance of 1212 and 813 F g^{-1} at the corresponding discharge current densities of 2 and 16 A g^{-1}.[37] From the date above, the α-$Ni(OH)_2$@HA nanotubes hybrid nanostructures show an enhanced electrochemical performance, which is ascribed to two main factors. First, the well-defined ultrathin standing and hierarchical nanosheets allow the materials to be in constant contact with electrolyte. This shortens the pathways of ions and incresed the availability of the nanostructures ensuring the good electrochemical performance of the supercapacitor. Second, the sufficient supply of hydroxyl groups and the remarkable cation/anion exchange capacity of HA increase the capacitance and stability of the supercapacitor from the chemical reaction kinetic point of view.

4. Conclusion

A new composite nanostructured material (α-$Ni(OH)_2$ nanosheets@HA) is developed to improve the electrochemical performance of supercapacitors. The material can be prepared by a simple, low-cost and green electrochemical process. Measurements show that the nanosheets, combined with with HA nanotubes, possess excellent electrochemical performance, such as high specific capacitance and long cycle life, and thus are suitable as advanced electrode materials for pseudo-supercapacitors. This demonstrated feature of α-$Ni(OH)_2$@HA hybrid nanostructures will promote new opportunities to make high–performance supercapacitors and other energy-storage devices. Using HA as a substrate, other materials (such as cobalt hydroxide, zinc hydroxide, nickel cobaltite and so on) may also be grown to form hybrid nanostrures for supercapacitor applications, which is under current study.

Acnowledgements

This research was supported partially by the National Natural Science Foundation of China (No. 51273158, 21303131); Natural Science Basis Research Plan in Shaanxi Province of China (No. 2012JQ6003, 2013KJXX-49); Ph.D. Programs Foundation of Ministry of Education of China (No. 20120201120048); Program for New Century Excellent Talents in University (NCET-13-0449). The authors are

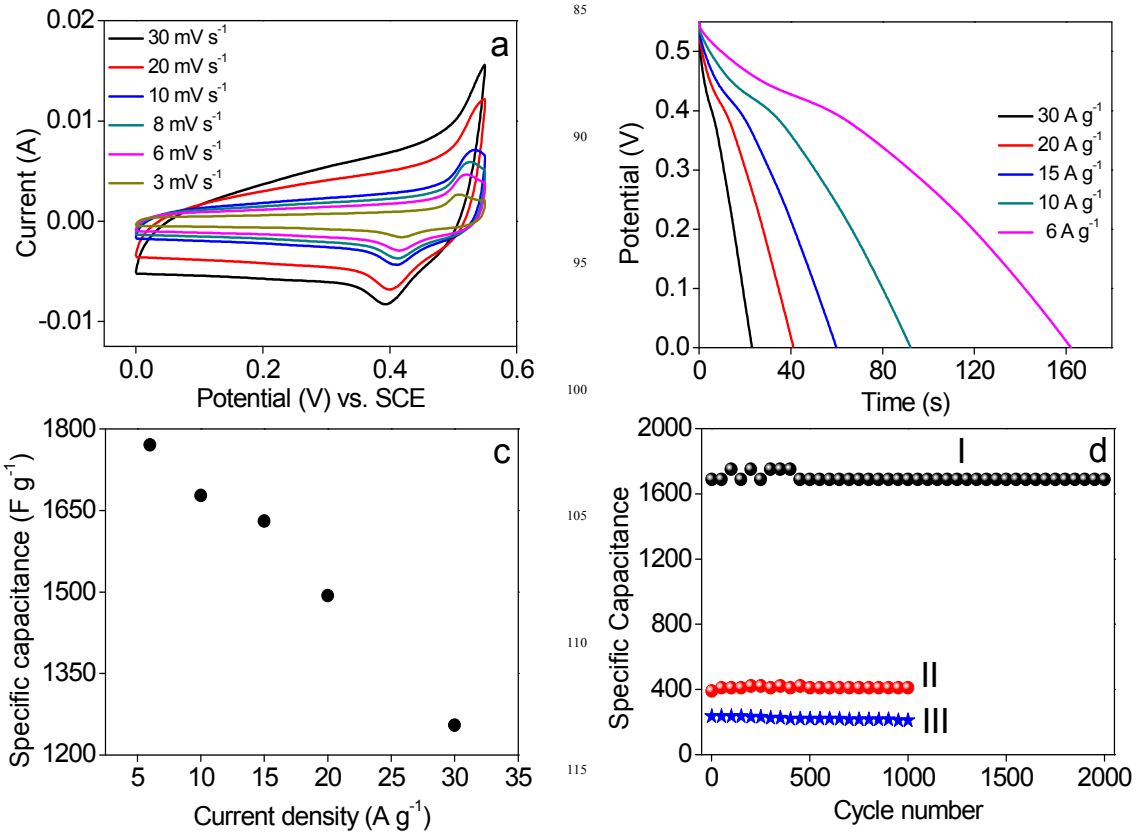

Fig. 7 Electrochemical characterizations of the α-$Ni(OH)_2$ nanosheets@HA. (a) CV curves at various scan rate ranging from 3 to 30 mV s^{-1}; (b) Charge/discharge voltage profiles at various current densities ranging from 6 to 30 A g^{-1}; (c) The calculated capacitance as a function of current density according to the data in (b); (d) The capacitance cycling performance at current density of 10 A g^{-1}: α-$Ni(OH)_2$ nanosheets@HA (I), α-$Ni(OH)_2$ (II) and HA nanotubes (III).

grateful to the Fundamental Research Funds for the Central Universities for financial support. We thank Prof. Chunming Niu for his valuable suggestions to our original manuscript.

Notes and references

[a] *State Key Laboratory for Mechanical Behaviour of Materials, MOE Key Laboratory for Nonequilibrium Synthesis and Modulation of Condensed Matter and Department of Applied Chemistry, School of Science, Xi'an Jiaotong University, Xi'an 710049, China. E-mail: dingsj@mail.xjtu.edu.cn*
[b] *The Department of Applied Chemistry, School of Chemical Science and Technology, Yunnan University, Kunming 650091, China. E-mail: licp830 @iccas.ac.cn*
[c] *State Key Laboratory for Manufacturing Systems Engineering, Xi'an Jiaotong University; Department of Mechanical Engineering, University of Michigan-Dearborn, Dearborn, MI 48128 USA, Xi'an 710049, PR China.*
[d] *The center of nanomaterials for renewable energy, Xi'an Jiaotong University, Xi'an, China.*
[e] *Electronic Materials Research Laboratory, Key Laboratory Of The Ministry Of Education & International Center For Dielectric Research, Xi'an Jiaotong University, Xi'an, China.*

1. M. Winter and R. J. Brodd, *Chem. Rev.*, 2004, **104**, 4245-4270.
2. A. S. Aricò, P. Bruce, B. Scrosati, J. Tarascon and W. Van Schalkwijk, *Nat. Mater.*, 2005, **4**, 366-377.
3. Y. G. Guo, J. S. Hu and L. J. Wan, *Adv. Mater.*, 2008, **20**, 2878-2887.
4. J. Jiang, J. P. Liu, W. W. Zhou, J. H. Zhu, X. T. Huang, X. Y. Qi, H. Zhang and T. Yu, *Energy Environ. Sci.*, 2011, **4**, 5000-5007.
5. X. Xu, J. Liang, H. Zhou, D. M. Lv, F. X. Liang, Z. L. Yang, S. J. Ding and D. M. Yu, *J. Mater. Chem. A*, 2013, **1**, 2995-2998.
6. G. Wang, L. Zhang and J. Zhang, *Chem. Soc. Rev.*, 2012, **41**, 797-828.
7. C. Liu, F. Li, L. P. Ma and H. M. Cheng, *Adv. Mater.*, 2010, **22**, E28-E62.
8. P. Simon and Y. Gogotsi, *Nat. Mater.*, 2008, **7**, 845-854.
9. J. R. Miller and P. Simon, *Science*, 2008, **321**, 651-652.
10. D. Bhattacharjya, M. S. Kim, T. S. Bae and J. Yu, *J. Power Sources*, 2013, **244**, 799-805.
11. P. Si, S. J. Ding, J. Yuan, X. W. Lou and D. H. Kim, *ACS nano*, 2011, **5**, 7617-7626.
12. G. Q. Zhang, H. B. Wu, H. E. Hoster, M. B. Chan-Park and X. W. D. Lou, *Energy Environ. Sci.*, 2012, **5**, 9453-9456.
13. G. Q. Zhang and X. W. D. Lou, *Adv. Mater.*, 2013, **25**, 976-979.
14. S. J. Ding, T. Zhu, J. S. Chen, Z. Y. Wang, C. L. Yuan and X. W. D. Lou, *J. Mater. Chem.*, 2011, **21**, 6602-6606.
15. W. J. Zhou, X. H. Cao, Z. Y. Zeng, W. H. Shi, Y. Y. Zhu, Q. Y. Yan, H. Liu, J. Y. Wang and H. Zhang, *Energy Environ. Sci.*, 2013, **6**, 2216-2221.
16. H. L. Wang, H. S. Casalongue, Y. Y. Liang and H. J. Dai, *J. Am. Chem. Soc.*, 2010, **132**, 7472-7477.
17. Z. Y. Lu, Z. Chang, W. Zhu and X. M. Sun, *Chem. Commun.*, 2011, **47**, 9651-9653.
18. B. P. Bastakoti, H. S. Huang, L. C. Chen, K. C. Wu and Y. Yamauchi, *Chem. Commun.*, 2012, **48**, 9150-9152.
19. H. L. Wang, Y. Y. Liang, T. Mirfakhrai, Z. Chen, H. S. Casalongue and H. J. Dai, *Nano Research*, 2011, **4**, 729-736.
20. B. J. Li, M. Ai and Z. Xu, *Chem. Commun.*, 2010, **46**, 6267-6269.
21. Y. X. Xu, Z. Y. Lin, X. Huang, Y. Liu, Y. Huang and X. F. Duan, *ACS nano*, 2013, **7**, 4042-4049.
22. S. S. Sun, C. C. Kong, S. Yang, L. Q. Wang, X. P. Song, B. Ding and Z. M. Yang, *CrystEngComm*, 2011, **13**, 2217-2221.
23. X. A. Chen, X. H. Chen, F. Q. Zhang, Z. Yang and S. M. Huang, *J. Power Sources*, 2013, **243**, 555-561.
24. D. G. Shchukin, G. B. Sukhorukov, R. R. Price and Y. M. Lvov, *Small*, 2005, **1**, 510-513.
25. C. P. Li, J. Q. Wang, S. Q. Feng, Z. L. Yang and S. J. Ding, *J. Mater. Chem. A*, 2013, **1**, 8045-8054.
26. E. Joussein, S. Petit and B. Delvaux, *Appl. Clay Sci.*, 2007, **35**, 17-24.
27. X. Xu, G. Yang, J. Liang, S. Ding, C. Tang, H. Yang, W. Yan, G. Yang and D. Yu, *Journal of Materials Chemistry A*, 2014, **2**, 116-122.
28. S. S. Sun, H. J. You, C. C. Kong, X. P. Song, B. J. Ding and Z. M. Yang, *CrystEngComm*, 2011, **13**, 2837-2840.
29. S. Shang, K. Xue, D. Chen and X. Jiao, *CrystEngComm*, 2011, **13**, 5094-5099.
30. J. Lang, L. Kong, W. Wu, M. Liu, Y. Luo and L. Kang, *J. Solid State Electr.*, 2009, **13**, 333-340.
31. D. Fix, D. V. Andreeva, Y. M. Lvov, D. G. Shchukin and H. Möhwald, *Adv. Funct. Mater.*, 2009, **19**, 1720-1727.
32. B. C. Guo, F. Chen, Y. D. Lei, X. L. Liu, J. J. Wan and D. M. Jia, *Appl. Surf. Sci.*, 2009, **255**, 7329-7336.
33. W. Huang, J. Zheng and Z. Li, *J. Phys. Chem. C*, 2007, **111**, 16902-16908.
34. J. W. Lee, T. Ahn, D. Soundararajan, J. M. Ko and J. Kim, *Chem. Commun.*, 2011, **47**, 6305-6307.
35. J. Yan, Z. J. Fan, W. Sun, G. Q. Ning, T. Wei, Q. Zhang, R. F. Zhang, L. J. Zhi and F. Wei, *Adv. Funct. Mater.*, 2012, **22**, 2632-2641.
36. J. Yan, W. Sun, T. Wei, Q. Zhang, Z. Fan and F. Wei, *J. Mater. Chem.*, 2012, **22**, 11494-11502.
37. Y. X. Xu, X. Q. Huang, Z. Y. Lin, X. Zhong, Y. Huang and X. F. Duan, *Nano Research*, 2013, **6**, 65-76.

Graphical Abstract

α-$Ni(OH)_2$ nanosheets@HA hybrid nanostructures exhibit an excellent specific capacitance and cycling stability at a high charge/discharge current density.